Investigation of charge trapping at the oxide/semiconductor interface for MBE-grown GaN films

J.C. Moore[a*], M.A. Reshchikov[b], J.E. Ortiz[b], J. Xie[c], H. Morkoç[c], A.A. Baski[b]
[a]Department of Chemistry and Physics, Longwood University, Farmville, VA 23901;
[b]Department of Physics and [c]Department of Electrical and Computer Engineering,
Virginia Commonwealth University, Richmond, VA 23284

ABSTRACT

Charge trapping resulting in localized band bending on MBE-grown GaN films was investigated using a new combination of conducting atomic force microscopy (CAFM) and scanning Kelvin probe microscopy (SKPM). CAFM was first used to locally inject charge at the surface oxide/semiconductor interface, and then SKPM was performed to monitor the evolution of the resulting surface potential. In a dark environment, the additionally charged interface states due to CAFM charge injection resulted in an induced additional band bending that persisted for hours. The induced band bending is nominal (<0.5 eV) for CAFM voltages less than 8 V, and reaches a saturation value of ~3 eV for voltages greater than 10 V. The saturation band bending corresponds to a total density of charged interface states (2×10^{12} cm^{-2}) that is double the value observed for the intrinsic surface. Induced band bending could still be observed up to 4 h after charge injection, indicating that charge trapping is relatively stable in a dark environment. However, charged interface states could be rapidly neutralized by illumination with UV light. A phenomenological model based on a tunneling mechanism was used to successfully describe the CAFM charge injection, where electrons travel from the tip through an oxide barrier and become trapped at oxide/GaN interface states. Saturation occurs due to the existence of a finite density of chargeable states at the interface. After charge injection, the decrease in induced band bending with time was found to be consistent with a thermionic model of charge transfer from the interface to the bulk.

Keywords: GaN, SKPM, CAFM, charge trapping, band-bending

1. INTRODUCTION

As is the case with many other semiconductors, undoped or *n*-type GaN exhibits strong upward band bending at the surface,[1] though there is still considerable debate over the responsible mechanism. Various studies of undoped *n*-type GaN films show band bending from 0.4 to 1.4 eV, with untreated surfaces closer to the high end of that range.[2,3,4,5] Spontaneous polarization along the [0001] direction has been proposed as one possible explanation for the observed band bending, though photoemission spectroscopy[6] and SKPM[7,8,9] studies of Ga- and N-polar GaN suggest that this may not be the case. Surface band bending has been shown to depend on the bulk concentration of free carriers, where SKPM measurements[9] and theoretical studies[10] show an increase in band bending with increased concentration of free electrons for MBE grown films. A process known as surface photovoltage has also been observed, where the migration of photogenerated holes to the surface and electrons to the bulk cause a reduction in the depletion layer electric field, thereby flattening the band bending. This effect has been theoretically described[1] and experimentally verified,[11] where photovoltages of 0.2 to 0.3 eV were observed with SKPM on GaN films.

Barriers formed by Schottky contacts can be affected by the presence of charged surface states, which could result in a degradation of electrical and optical properties for optoelectronic devices. Such concentrations of charged surface states have been linked to current collapse in GaN field effect transistors (FETs)[12] and power degradation in HFETs.[13,14] Therefore, understanding surface charging and related band-bending on GaN surfaces is of practical importance. It has been shown that a method based on SKPM can result in direct measurements of surface potential, which can be used to calculate surface band bending.[9] Although there are a considerable number of SKPM studies of GaN reported in the literature, there are no reported studies where SKPM is combined with CAFM to study GaN surface charging. In our studies we combine these techniques, using CAFM to charge the surface and SKPM to probe the resulting surface potential.

* moorejc@longwood.edu; phone 434-395-2577; fax 434-395-2652

Gallium Nitride Materials and Devices III, edited by Hadis Morkoç, Cole W. Litton, Jen-Inn Chyi, Yasushi Nanishi, Euijoon Yoon, Proc. of SPIE Vol. 6894, 68940B, (2008) · 0277-786X/08/$18 · doi: 10.1117/12.768041

2. EXPERIMENTAL

2.1 Sample Growth and Characterization

The GaN samples in this study consist of films grown by molecular beam epitaxy (MBE) on templates (1-2 μm thick) prepared by metal-organic chemical vapor deposition (MOCVD) on sapphire substrates. For MBE growth, the Ga source consisted of two double-zone Ga cells, and nitrogen was supplied by an RF plasma source. Before loading into the MBE chamber, the templates were cleaned by HNO3:HCl (1:3) acid (100 °C, 20 min). The films were grown under Ga-rich conditions with substrate temperatures of 650 to 700 °C. After opening the Ga cell shutters for 10 s, the nitrogen RF source was opened with a power setting of 300 W. Typical growth rates were 200 to 300 nm/hr, where a 1×1 RHEED pattern was observed for Ga-rich growth conditions.

2.2 Electronic Pump-Probe Microscopy

To learn more about the surface charging behavior of GaN, we have employed a new technique that we call electronic pump-probe microscopy (EPPM). Similar to more common optical pump-probe techniques, in EPPM the surface is "pumped" with charge via CAFM and then the local surface potential is "probed" using SKPM. Unlike optical techniques, EPPM allows for the characterization of highly localized regions (< 200 nm). However, one important drawback to EPPM is that the created charged surface states must be relatively stable, since pumping is temporally separated from probing by at least several minutes.

Figures 1(a) and (b) show a contact mode AFM image and a simultaneously acquired, reverse-bias CAFM current map, respectively, taken after several scans. Reverse-bias current leakage is visible in Fig. 1(b); however, the magnitude of leakage is reduced (compared to previous scans not shown) due to the growth of oxide islands (white bumps) on defective hillocks as seen in Fig. 1(a). Initially, it was our intention to study whether local charge trapping occurred for defective regions. To determine this we conducted SKPM experiments in the same region as initially scanned via CAFM. It is important to point out that all experiments (unless otherwise noted) were performed in a dark environment. Figure 1(c) shows a tapping-mode AFM image where the initial CAFM scanned region can be seen (highlighted by the white dotted box). Figure 1(d) shows the corresponding SKPM surface potential map, where a significant difference in contact potential (~3 V) is observed for scanned regions vs. unscanned regions. No local differences in surface potential are observed for current leakage defect regions.

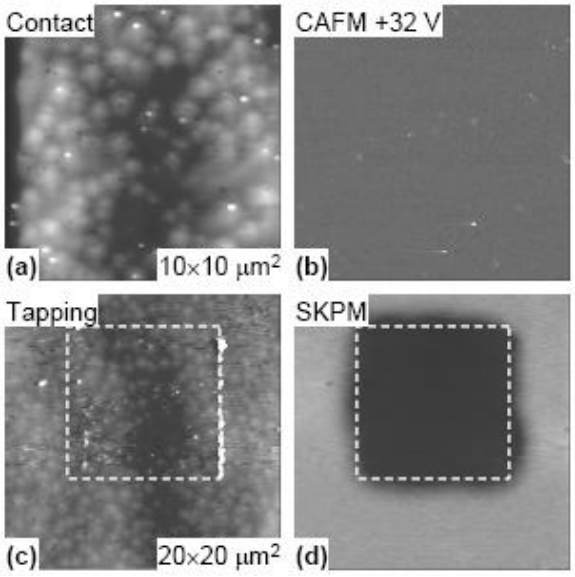

Figure 1: (a) Contact-mode topography image (grayscale range = 15 nm) of an MBE on MOCVD GaN surface with a (b) simultaneously acquired, reverse-bias CAFM current map (grayscale range = 50 nA). In the same region, a (c) tapping-mode topography image (grayscale range = 30 nm) is shown with the (d) corresponding SKPM surface potential map (grayscale range = 5 V). The dotted white boxes in (c) and (d) highlight the region initially scanned with CAFM.

2.3 Photosensitivity of the Charged Surface

The observed difference in local contact potential is sensitive to UV illumination. To study the photosensitivity of GaN surface charging, we used a 377 nm UV pulsed laser to illuminate our samples during characterization. Figure 2(a)

shows a SKPM surface potential map. The area highlighted by the dotted white lines indicates the region previously scanned at 12 V with CAFM. As expected, a 3 V difference in potential between the scanned and unscanned regions is observed. After acquisition of the image shown in Fig. 2(a), the surface was then illuminated with a UV laser. Immediately after illumination, Fig. 2(b) was acquired. Importantly, there is no difference in potential observed between the scanned and unscanned regions after illumination with UV light.

A similar sequence of images is shown in Figs. 2(c) and (d), where the surface is illuminated with a 15 W fluorescent bulb rather than a UV laser. Figure 2(c) shows a SKPM surface potential map. The area highlighted by the dotted white lines indicates the region previously scanned at 12 V with CAFM. In this case, a 1.5 V difference in potential between the scanned and unscanned regions is observed, which may be due to an increased elapsed time between the CAFM scan and the acquisition of SKPM data. Similar to the UV laser illumination, there is no difference in potential seen between the scanned and unscanned regions after illumination with a fluorescent bulb as shown in Fig. 2(d). Although illumination by a UV laser or fluorescent bulb both neutralize surface charging, the fluorescent bulb requires approximately 30 s to reach $\Delta V_{SP} = 0$, whereas the UV laser requires less time than measurable with the technique (<5 s).

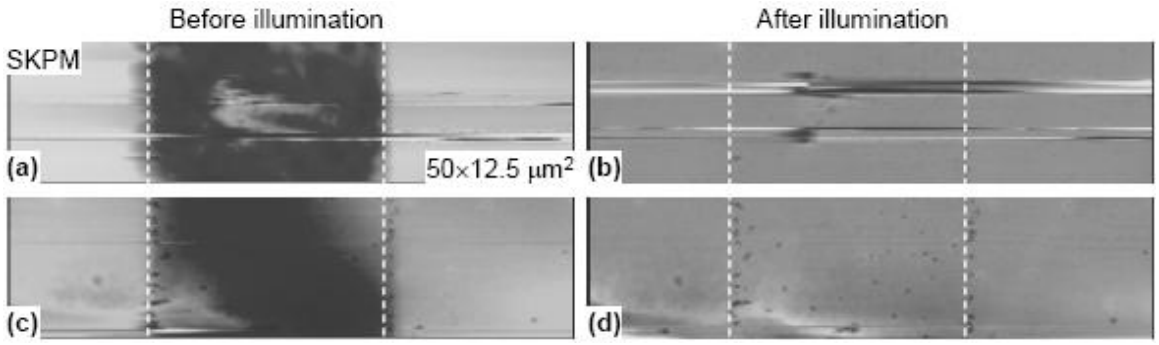

Figure 2: (a) SKPM surface potential map (grayscale range = 5 V) of MBE grown GaN on MOCVD after +12 V CAFM scan was performed in the region highlighted by white dotted lines. (b) Corresponding SKPM surface potential map acquired immediately after the surface was illuminated with a UV laser. (c) SKPM surface potential map (grayscale range = 2 V) of MBE grown GaN on MOCVD after +12 V CAFM scan was performed in the region highlighted by white dotted lines. (b) Corresponding SKPM surface potential map acquired immediately after the surface was illuminated with a 15 W fluorescent bulb.

Since the UV laser produces photons with an energy (3.7 eV) that is greater than the band gap of GaN (3.4 eV), electron-hole pairs are created within the depletion layer. The UV light is absorbed within the depletion layer where electrons are promoted from the valence band into the conduction band. Due to the electric field within the depletion layer, electrons and holes separate. Electrons travel into the bulk, whereas holes travel to the surface where they can recombine with electrons in surface states. This surface recombination results in a decrease in surface charging and band bending, and is observed in SKPM surface potential maps like those shown in Figs.2(b) and (d).

The fluorescent bulb discussed above emits some UV radiation, though with a lower intensity compared to the UV laser. The laser used in this study produces approximately 4×10^{14} photons/cm^2 during every pulse. As discussed below, there is a surface charge density of ~2×10^{12} cm^{-2} when charged via CAFM at biases greater than 12 V. Since the adsorption process within the depletion layer is very efficient, without attenuation one pulse should neutralize all charge within the scanned regions, which is consistent with our measurements.

3. SURFACE CHARGING AND BAND-BENDING

The electric field resulting from trapped negative charge on a surface causes an upward shift in energy levels. This bending of potentials near the surface causes free electrons to move away from the surface into the bulk, leaving a depletion layer with a width (W_0) of approximately 100 nm (for $n_0 \approx 10^{17}$ cm^{-3}). The magnitude of the shift in energy levels is called the band bending (ϕ_0), which can be found as:[11]

$$\phi_0 = \phi_M - qV_{SP} - \phi_s - \chi + E_F \quad (1),$$

where ϕ_M is the metal work function, V_{SP} is the surface contact potential, ϕ_s is the potential drop across the oxide film, χ is the electron affinity of the semiconductor, and E_F is the Fermi level. Previous SKPM studies have determined $\phi_0 \approx 1$ eV for the types of films investigated in this study.[8] The depletion layer width can then be determined from the band bending and the concentration of shallow donors (N_D) as follows:

$$W_0 = \sqrt{\frac{2\phi_0 \varepsilon \varepsilon_0}{qN_D}} \tag{2}.$$

As determined by Hall effect measurements, our GaN samples have a concentration of free electrons (which is close to N_D in the first approximation) of approximately 10^{17} cm^{-3}, which results in a native depletion layer width of ~100 nm.

If more charge becomes trapped on the surface, then the increase in electric field increases the width of the depletion layer. In this case, the depletion layer width (W_{CAFM}) and band bending ($\phi_0 + \Delta\phi_{CAFM}$) is increased due to the increase in electric field caused by trapped electrons at the surface. We can relate the increase in band bending ($\Delta\phi_{CAFM}$), which we observe as $q\Delta V_{SP}$ in SKPM measurements, to the depletion layer width as follows:

$$W_{CAFM} = \sqrt{\frac{2(\phi_0 + \Delta\phi_{CAFM})\varepsilon \varepsilon_0}{qN_D}} \tag{3}.$$

From our SKPM measurements, $\Delta\phi_{CAFM} \approx 3$ eV for applied CAFM biases $V_{CAFM} > 9$ V, which results in a depletion layer width of $W_{CAFM} \approx 200$ nm, or twice the width of the native depletion layer. The density of charged surface states for the unscanned (N_{SS_0}) and scanned ($N_{SS_{CAFM}}$) regions can be estimated as:

$$N_{SS_0} = W_0 N_D = 1 \times 10^{12} cm^{-2} \tag{4},$$

and

$$N_{SS_{CAFM}} = W_{CAFM} N_D = 2 \times 10^{12} cm^{-2} \tag{5},$$

implying that applied CAFM biases greater than 9 V result in a doubling of charged surface state density. Similarly, the electric field within the depletion region (E_0) can be shown to double with deposition of charge via CAFM (E_{CAFM}):

$$E_0 = \frac{\phi_0}{W_0} = 1 \times 10^5 \frac{V}{cm} \tag{6},$$

and

$$E_{CAFM} = \frac{\phi_0 + \Delta\phi_{CAFM}}{W_{CAFM}} = 2 \times 10^5 \frac{V}{cm} \tag{7}.$$

3.1 Band-Bending as a Function of CAFM Applied Bias

The difference in band bending between the scanned and unscanned region ($\Delta\phi_{CAFM}$) depends on the bias applied during the CAFM scan (V_{CAFM}), as seen in Fig. 3. There is a sharp increase in $\Delta\phi_{CAFM}$ at V_{CAFM} = ~5 V that quickly reaches a saturation value of approximately 3 V for an applied bias of V_{CAFM} = 9 V, with no further increase in surface potential difference observed for applied biases up to at least 32 V. This dependence may initially be surprising; however, this behavior can be explained if an insulating barrier is assumed to exist between the tip and the GaN layer, and that the density of charged states reaches saturation. Previous studies indicate that the GaN surface is covered by a native oxide with a thickness of at least 1 nm, which may act as an insulating layer.[15] When a bias is applied to the surface via CAFM, a breakdown occurs and electrons can penetrate the oxide layer and travel to the oxide/GaN interface where they can be trapped in GaN interface states. To approximate this behavior, we assume that the electron current through the insulating layer is exponentially dependent on the applied bias. The density of charged surface states N_{SS} is then given by:

$$N_{SS} = \beta(N_{SS_{\max}} - N_{SS}) e^{\alpha(qV_{CAFM})} \tag{8},$$

where $N_{SS_{\max}}$ is the maximum density of surface states that can trap electrons. The proportionality constants α and β can be determined from the boundary condition at $V_{CAFM} = 0$ where N_{SS} is equal to the native density of charged states N_{SSo}. Applying this condition to Eq. (8) yields the following:

$$N_{SS_0} = \beta\left(N_{SS_{\max}} - N_{SS_0}\right) \tag{9},$$

such that

$$\beta = \frac{N_{SS_0}}{N_{SS_{\max}} - N_{SS_0}} \tag{10}.$$

Inserting Eq. (10) into Eq. (8) yields:

$$\frac{N_{SS}}{N_{SS_0}} = \frac{N_{SS_{\max}}}{N_{SS_0} + \left(N_{SS_{\max}} - N_{SS_0}\right)e^{-\alpha(qV_{CAFM})}} \tag{11},$$

which shows that the density of charged surface states is a sigmoid function of V_{CAFM}. Our experimentally obtained value for the difference in band bending ($\Delta\phi_{CAFM}$) can be related to Eq. (11) since

$$\Delta\phi_{CAFM} = \phi - \phi_0 \tag{12},$$

and

$$\phi = \phi_0\left(\frac{N_{SS}}{N_{SS_0}}\right)^2 \tag{13}.$$

Substituting Eqs. (12) and (13) into Eq. (11) yields the following expression for the change in band bending induced by CAFM as a function of applied bias V_{CAFM}:

$$\Delta\phi_{CAFM} = \phi_0\left\{\frac{N_{SS_{\max}}^2}{\left[N_{SS_0} + \left(N_{SS_{\max}} - N_{SS_0}\right)e^{-\alpha(qV_{CAFM})}\right]^2} - 1\right\} \tag{14}.$$

Our data shown in Fig. 3 were fit to Eq. (14), as shown by the dotted line, where $N_{SS_{\max}} = 2\times10^{12}$ cm^{-2}, $N_{SS_0} = 1\times10^{12}$ cm^{-2}, and $\phi_0 = 1$ eV. The fitting parameter α was varied until a reasonable fit was achieved at $\alpha = 0.25$ eV^{-1}, which is an acceptable value for room temperature experiments. Although a qualitative fit of the data is observed, avalanche breakdown should dominate conduction through the barrier at larger biases. Therefore, our model is an approximation that suggests an insulating barrier exists between the CAFM tip and GaN film, and that the density of charged states eventually reaches saturation.

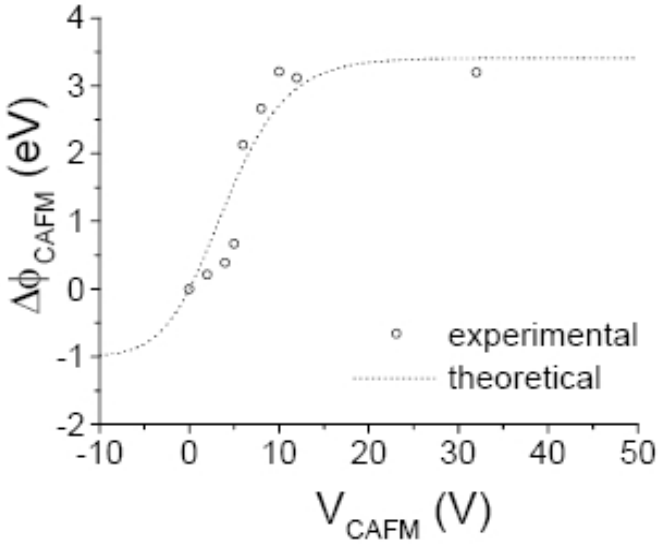

Figure 3: Plot of measured difference in surface potential between scanned and unscanned regions ($\Delta\phi_{CAFM}$) as a function of applied bias (V_{CAFM}) in CAFM. The dotted line shows the best fit curve calculated using Eq. 14.

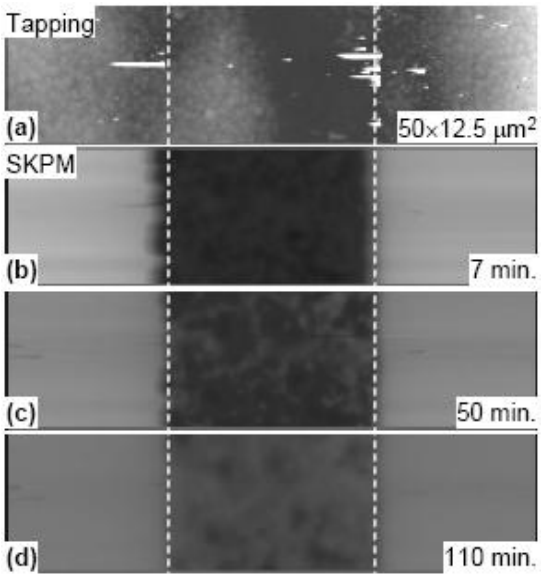

Figure 4: (a) Tapping-mode AFM topography image (grayscale range = 50 nm) of MBE grown GaN on MOCVD with corresponding SKPM surface potential maps (grayscale range = 8 V) obtained at (b) 7 minutes, (c) 50 minutes, and (d) 110 minutes.

3.2 Band-Bending as a Function of Discharge Time

To study the stability of charge trapping on GaN surfaces, we have also examined the change in band bending with time after the completion of charge injection. Figure 4(a) shows a tapping-mode image of the GaN surface with a region previously scanned at 12 V CAFM highlighted by the white dotted lines. Corresponding SKPM images at various times after the CAFM scan are shown in Figs. 4(b) to (d). Times quoted are the time from the completion of the CAFM scan to the time of the start of the image presented. It takes approximately 7 min from the completion of the CAFM scan to change the tip for SKPM and re-approach in the same area. The difference in surface potential between the scanned and unscanned regions decreases with time, indicating discharging of the surface. Interestingly, the scanned/unscanned region boundary remains sharp throughout the discharging process, indicating that charge does not move laterally across the surface and that charge neutralization occurs via a transfer of electrons from the surface to the bulk.

A plot of the measured difference in band bending between scanned and unscanned regions as a function of time is shown in Fig. 5. Data presented as hollow circles were acquired sequentially, i.e., SKPM imaging was done continuously. From this plot, it can be seen that surface charge trapping is relatively stable, with a relatively significant amount of band bending still visible up to 4 hours after the deposition of charge. To determine whether the surface is discharged through the AFM tip during imaging, we also acquired data at specific time intervals (filled circles). Since there is no observable difference between the two curves, we conclude that any discharge due to the tip's contact with the surface is negligible.

The difference in band bending is quasi-exponential in time. A similar type of behavior is seen in photovoltage studies where band bending is reduced via illumination. Surface charge is restored via thermionic transfer of free electrons from the bulk to the surface states over the near-surface barrier.[11] We speculate that a similar mechanism may be responsible for the discharging behavior here, though in our case, the dominant transfer of electrons is from surface states to the bulk. The dynamics of this transfer is determined by the following rate equation:

$$\frac{\partial N_{SS}}{\partial t} = -AN_{SS} + S(t) \qquad (15),$$

with $$A = c_n N_C e^{\frac{-E_{SS}}{kT}} \quad (16),$$

and $$S(t) = N_D N_{SS}^* c_n e^{\frac{-\phi(t)}{kT}} \quad (17),$$

where N_{SS} and N_{SS}^* are the densities of negatively charged and neutral surface states at an arbitrary time, respectively, c_n is the electron capture coefficient for the surface states,[16] N_C is the density of states in the conduction band, and E_{SS} is the absolute value of the surface state energy level with respect to the conduction band. Physically, the first term on the right hand side of Eq. (15) represents charge transfer from the surface states to the bulk and the second term represents charge transfer from the bulk to the surface states. The emission coefficient A is time independent, whereas the capture rate $S(t)$ is exponentially dependent on time since the total band bending ϕ decreases as electrons are transferred. In principle, the concentration of available surface states for electrons N_{SS}^* may be time dependent as well.

Equation (15) cannot be solved analytically. To obtain an approximate solution, we ignore $S(t)$ and assume that only excess electrons ($N_{SS} - N_{SS_0}$) are available to escape, i.e.,

$$\frac{\partial N_{SS}}{\partial t} = -A\left(N_{SS} - N_{SS_0}\right) \quad (18).$$

Such an approximation is justified since for small values of t, $\phi >> E_{SS}$ such that the first term on the right-hand side of Eq. (15) dominates. However, for sufficiently large t, escape of electrons from the surface to the bulk becomes comparable to the capture of electrons by the surface from the bulk, which results in a failure of the approximation. Therefore, our model is an approximation for relatively small values of t. The solution to Eq. (18) is:

$$N_{SS} = \alpha e^{-At} + \beta \quad (19).$$

To determine the constants α and β, we consider the boundary conditions as $t \to \infty$, where the concentration of charged surface states approaches the native concentration of charged surface states for GaN, and at $t = 0$, where the concentration of charged surface states is equal to the concentration of charged surface states after charge injection via CAFM:

$$t \to \infty, \quad N_{SS} = N_{SS_0}$$
$$t = 0, \quad N_{SS} = N_{SS_{CAFM}}$$

By applying these boundary conditions, the solution becomes

$$\frac{N_{SS}}{N_{SS_0}} = \left(\frac{N_{SS_{CAFM}}}{N_{SS_0}} - 1\right)e^{-At} + 1 \quad (20).$$

Equation (20) can be related to the experimentally obtained value $\Delta\phi_{CAFM}$ by substituting Eqs. (12) and (13) and yields:

$$\Delta\phi_{CAFM} = \phi_0 \left\{\left[\left(\frac{N_{SS_{CAFM}}}{N_{SS_0}} - 1\right)e^{-At} + 1\right]^2 - 1\right\} \quad (21).$$

Our data for surface discharging with time were fit to Eq. (21) for relatively small values of t (as shown by the dotted line in Fig. 5), where an assumed value of ϕ_0 = 1.0 eV [5] yields an emission coefficient $A = 1.8\times10^{-4}$ sec^{-1} and ratio $N_{SSCAFM}/N_{SSo} = 2.06$. Deviation from the fit at large t is due to our approximation; however, for $t < 10^4$ s this model gives a reasonable fit. Although the emission coefficient is estimated, the capture coefficient c_n and position of the surface state energy level E_{SS} cannot be determined from our room-temperature data. However, from the obtained emission coefficient

A we can estimate that E_{SS} = 0.5–1.0 eV for a range of reasonable c_n values (10^{-14}-10^{-5} cm^3/s).[16] In order to determine the values of E_{SS} and c_n, temperature-dependent measurements are necessary. Thus, this phenomenological model explains the dynamics of injected surface charge neutralization with time.

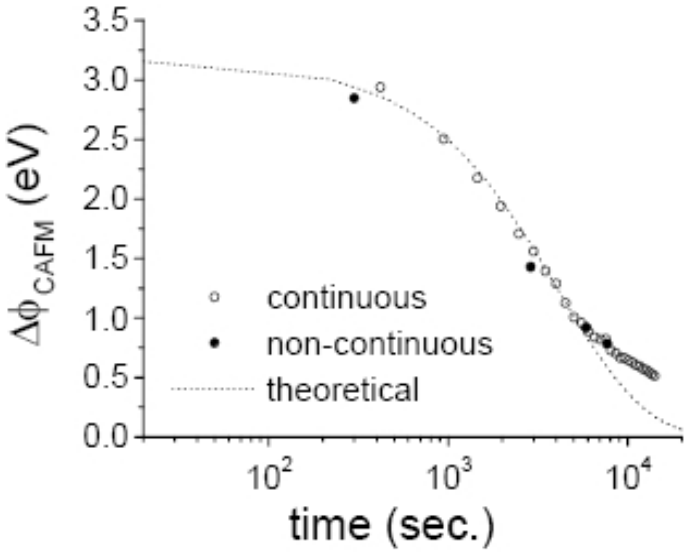

Figure 5: Plot of measured difference in surface potential between scanned and unscanned regions ($\Delta\phi_{CAFM}$) as a function of time. Continuously acquired data is shown as hollow circles and data acquired non-continuously are shown as filled circles. The dotted line shows the best fit curve calculated using Eq. 21.

4. CONCLUSIONS

In conclusion, we have presented a new technique for studying charged surface states. The combination of CAFM and SKPM (which we have termed EPPM) was used to examine surface state charging in MBE grown GaN films on MOCVD templates. Although we found no discernable difference in surface potential after charging between localized defective regions and non-defective regions, we did observe an overall increase in surface charge (and therefore band bending) in regions scanned via CAFM. We developed two phenomenological models that suggest the following: (1) charge trapping occurs at the interface between an insulating layer and GaN, (2) saturation of charged states occurs with increased CAFM applied bias, and (3) injected charge is slowly neutralized via thermionic emission of electrons from the interface to the bulk. Calculated values for native band bending and the capture coefficient were in good agreement with previous studies. As expected, charged states could also be neutralized more rapidly via photovoltage caused by illumination with UV light. EPPM offers a relatively simple method for determining native band bending on semiconductor surfaces and could become a useful tool for measuring the concentrations of surface states.

REFERENCES

1. W. Mönch, *Semiconductor Surfaces and Interfaces*, Springer, Berlin (1993).
2. V. M. Bermudez, *J. Appl. Phys.* **80**(2), 1190 (1996).
3. C. I. Wu, A. Kahn, N. Taskar, D. Dorman, D. Gallagher, *J. Appl. Phys.* **83**(8), 4249 (1998).
4. C. I. Wu, A. Kahn, *J. Vac. Sci. Technol. B* **16**(4), 2218 (1998).
5. S. Sabuktagin, M. A. Reshchikov, D. K. Johnstone, and H. Morkoc, *Mater. Res. Soc. Symp. Proc.* **798**, Y5.39 (2004).
6. H.W. Jang, K.W. Ihm, T-H Kang, J-H Lee, J-L Lee, *Phys. Stat. Sol. (b)* **240**, 451 (2003).
7. B. J. Rodriguez, W.-C. Yang, R. J. Nemanich, and A. Gruverman, *Appl. Phys. Lett.* **86**, 112115 (2005).
8. S. Sabuktagin, M.A. Reshchikov, D.K. Johnstone, H. Morkoç, *Mat. Res. Soc. Symp. Proc.* **798**, Y5.39.1 (2004).

9. K.M. Jones, P. Visconti, F. Yun, A.A.Baski, H. Morkoç, Appl. Phys. Lett. **78**, 2497 (2001).
10. K.A. Bulashevich, S.Yu. Karpov, *Phys. Stat. Sol. (c)* **3**, 2356 (2006).
11. M. A. Reshchikov, S. Sabuktagin, D.K. Johnstone, H. Morkoç, *J. Appl. Phys.* **96**(5), 2556 (2004).
12. G. Koley, V. Tilak, L.F. Eastman, M.G. Spencer, *IEEE Trans. Electr. Dev.* **50**(4), 886 (2003).
13. S. Sabuktagin, Y.-T. Moon, S. Dogan, A.A. Baski, H. Morkoç, *IEEE Electr. Dev. Lett.* **27**(4), 211 (2006)
14. W.S. Tan, M.J. Uren, P.A. Houston, R.T. Green, R.S. Balmer, T. Martin, *IEEE Electr. Dev. Lett.* **27**(1), 1 (2006).
15. T. Sasaki, T. Matsuoka, *J. Appl. Phys.* **64**, 4531 (1988).
16. M.A. Reshchikov, H. Morkoç, *J. Appl. Phys.* **97**, 061301 (2005).